A Simulink Model for the Dynamic Analysis of Floating Wind Turbines

Jiayao Meng[1], Ross A. McAdam[2], and Manolis N. Chatzis[1]

[1]Department of Engineering Science, University of Oxford, Parks Road, OX1 3PJ Oxford, UK
[2]Ørsted Power (UK), 5 Howick Place, SW1P 1WG London, UK

ABSTRACT

The drive to maximize the wind-energy harnessing capabilities of modern societies is gradually leading towards the design of floating wind turbines (FWT). To guide such designs, accurate numerical models that predict the dynamic behavior of the systems are crucial to ensure their structural reliability. This work presents a new Simulink implementation of the FWT modeling with a focus on the wave-platform interaction. The hydrostatic and hydrodynamic forces applied to the floating platform are calculated using a numerical and an analytical approach. The numerical approach makes use of the open-source Boundary Element Method (BEM) code, Nemoh. In the analytical approach, which is initially limited to a planar response of the FWT, a matched eigenfunction expansions method is examined to evaluate closed-form solutions of the velocity potential and the resulting force. This second approach offers deeper insights into the dynamic system and potentially higher computational efficiency compared to Nemoh. Both approaches are implemented as Simulink subsystems that are integrated with the remaining system in the time domain. The large variety of libraries in Simulink also enables the detailed modeling of other physics including aerodynamics, structural dynamics, and controls. The aerodynamic loads are applied at different cross-sections along the blade using the unsteady blade/element momentum method. While their flexibility can be accounted for, the blades and tower are modeled as rigid bodies in the present study and the effect of the mooring lines is taken into account as a resulting stiffness matrix. The industry-standard ROSCO controller is also employed. Validation against the most popular tool OpenFAST is carried out on the 5-MW ITIBarge FWT, and the overall agreement demonstrates the capability of the developed Simulink model to perform accurate dynamic analysis for FWTs.

Keywords: FWT, modeling, dynamics, Simulink, offshore

INTRODUCTION

Offshore wind energy has the potential of meeting the total world's electricity demand and could contribute significantly to achieving the target of limiting global temperature rise to 1.5°C by 2050 [1]. Around 80% of the offshore wind resource is in waters deeper than 60 m, where the deployment of bottom-fixed offshore wind turbines may not be economically viable. Floating wind turbines (FWT), which are relatively insensitive to water depth, provide promising alternatives to harness substantial offshore wind resources in deep waters far from the shore. However, the contradictory objectives of structural safety under the harsh ocean environment and of competitive cost-of-energy to attract market investments bring about great difficulties in the FWT design. The reliable and cost-effective design of FWTs is one of the key drivers to unleash the offshore wind potential.

A reliable design of the FWT should ensure the structural integrity and serviceability under the combined effects of gravitational and inertial loads, aerodynamic loads, hydrodynamics loads, mooring loads, and ice loads (where applicable) [2]. The comparison to field measurements is the most direct means of validating a FWT's design concept, and it has been deployed in the "Hywind Demo" and "Hywind Scotland" projects [3, 4]. However, in parallel to such experimental data, numerical modeling of such structures needs to be further developed. In light of this, simulation tools which can perform fully-coupled aero-hydro-elastic dynamic analysis are highly demanded. Several popular simulation tools are available for the dynamic analysis of FWTs, e.g. OpenFAST [5], Bladed [6], and HAWC2 [7]. Code-to-code, as well as code-to-experiment verifications, have been inves-

tigated through a series of projects led by the NREL (the phase IV of OC3 [8], phase II of OC4 [9], phase II of OC5 [10], and phase I of OC6 [11]). Despite each of these codes providing a reasonable representation of various domains of the problem, each of them makes use of a different set of assumptions, and some of the aforementioned codes are not open-source. The advantage of a code developed entirely in MATLAB/Simulink has the potential of easily integrating the multi-physics toolboxes developed by the multiple different communities working on the problem of estimating the overall performance of FWTs.

In this work the tower of the FWT is assumed to be fixed on a floating platform. The movement of this platform has a strong influence on the overall dynamic performance of the system. Therefore, the accurate description of the wave-body interaction problem is crucial for the coupled dynamic analysis of FWTs. The BEM codes, e.g. WAMIT [12], AQWA [13], Nemoh [14], are commonly used to calculate the hydrodynamic forces for the dynamic analysis of FWTs in popular tools (e.g. OpenFAST). BEM codes are of advantage when dealing with the floating platform of arbitrary geometries. As an alternative, the analytical approach employing the separation of variables and eigenfunction expansion matching methods, can provide closed-form solutions to the wave-platform boundary value problem (BVP) [15]. It offers deeper insights into the dynamic system and potentially higher computational efficiency compared to the numerical method, which solves the BVP by discretizing the calculation region. Both methods are studied in the present work to provide hydrodynamic coefficients for the FWT modeling.

In this conference paper, the tower, hub, nacelle and platform are modeled as single rigid bodies separately, the blade is modeled as a sequence of rigid bodies with distributed masses and inertias, and the mooring system is represented with a stiffness matrix in Simulink. The aerodynamic loads calculated by the unsteady dynamic blade element/momentum method [16] and the hydrodynamic loads determined by both numerical (Nemoh) and analytical methods are integrated into the Simulink model. The industry-standard ROSCO controller [17] is implemented in the model to regulate the power generation. The 5-MW ITIBarge FWT is taken as an example to validate the analytical wave-platform interaction modeling approach as well as the Simulink implementation of the FWT system. The hydrodynamic loads calculated from the analytical approach are shown in the example to compare well with those obtained from Nemoh. The dynamic responses of both Simulink-Nemoh and Simulink-Analytical models are also shown to be in good agreement with the OpenFAST-Nemoh model, which indicates the capability of the developed model in Simulink to accurately capture FWT dynamics.

WAVE-PLATFORM INTERACTION MODELING

Two right-handed Cartesian coordinate systems are defined to describe the 3D movements of a FWT platform as well as the wave kinematics in an open sea of finite depth H (as shown in Fig.1). Let O be the intersection point of the tower centerline and the mean free wave surface when the FWT is in an equilibrium position. The coordinate system $OXYZ$ is earth-fixed with the plane OXY lying on the mean free surface, OX pointing downwind, and OZ pointing upwards. The other coordinate system $O'X'Y'Z'$ is fixed on the platform and coincident with $OXYZ$ when there is no perturbation. The translational displacement from O to O' in the surge, sway, and heave Degree of Freedom (DoF) is denoted as ξ_1, ξ_2, ξ_3, respectively, and the rotation of roll, pitch and yaw DoF as ξ_4, ξ_5, ξ_6, respectively, with the Euler angle sequence being Cartesian $X \rightarrow$ rotated Y following the ξ_4 transformation $\rightarrow$ rotated Z following the ξ_4 and ξ_5 transformations, as shown in Fig.1.

Equations of the Boundary Value Problem (BVP)

Ideal fluid (homogeneous, inviscid, and incompressible) without rotational motion and surface tension is assumed here, in which case the flow can be completely described by a velocity potential $\Phi(x, y, z, t)$ satisfying Laplace's equation

$$\nabla^2 \Phi = 0, \tag{1}$$

where $\nabla^2 = \frac{\partial^2}{\partial x^2} + \frac{\partial^2}{\partial y^2} + \frac{\partial^2}{\partial z^2}$, throughout the whole domain Ω enclosed by the free surface S_F, body surface S_B, sea bottom S_D, and far-field boundary S_∞ (see Fig.1). The fluid pressure $p(x, y, z, t)$ can be obtained from Bernoulli's equation

$$p = -\rho \frac{\partial \Phi}{\partial t} - \frac{1}{2}\rho(\nabla \Phi)^2 - \rho g z, \tag{2}$$

where ρ is the fluid density and g the gravitational acceleration. By assuming small wave amplitudes relative to the wavelength, and small displacements and rotations of the platform relative to the platform characteristic dimension, the BVP that Φ should satisfy can be linearized on the still water level ($\overline{S}_F$) and mean wetted body surface ($\overline{S}_B$). This simplification allows for the decomposition of Φ into an incident wave potential Φ_I, radiation potential Φ_R and diffraction potential Φ_D. Φ_R handles the nonhomogeneous body surface boundary condition, Φ_I is an exogenous input to the fluid-body system and Φ_D is used to cancel
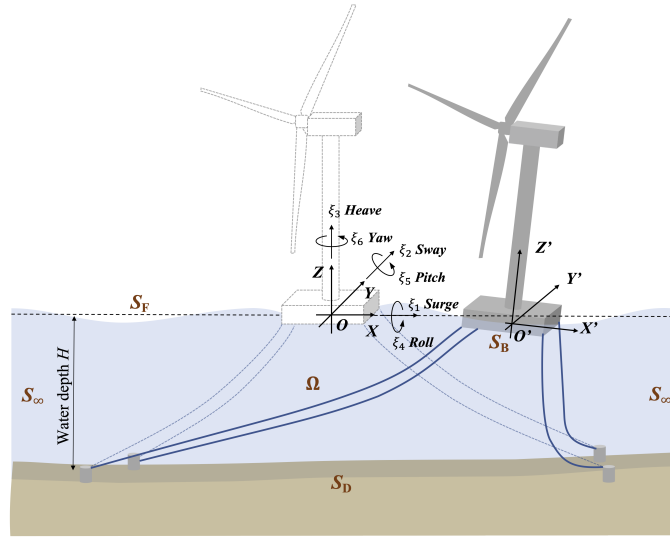
Figure 1: Coordinate system of a floating wind turbine. Only 6 platform DoFs are shown here.

out the influence of Φ_I onto the body surface. The total velocity potential can be written as

$$
\begin{aligned}
\Phi(x,y,z,t) &= \Phi_R(x,y,z,t) + \Phi_I(x,y,z,t) + \Phi_D(x,y,z,t) \\
&= \Re \left\{ \frac{1}{2\pi} \int_{-\infty}^{\infty} \left\{ \overline{\mathbf{V}}(\omega) \cdot \boldsymbol{\phi}_R(x,y,z,\omega) + \overline{\eta}(\omega) \left[\phi_I(x,y,z,\omega) + \phi_D(x,y,z,\omega) \right] \right\} e^{i\omega t} \, d\omega \right\},
\end{aligned}
\tag{3}
$$

where $\boldsymbol{\phi}_R$ is the radiation wave potential vector corresponding to different platform DoFs, which is, however, independent of the platform velocity; ϕ_I, ϕ_D are the incident and diffraction wave potential, respectively, and they are independent of the wave elevation; $\overline{\mathbf{V}}(\omega), \overline{\eta}(\omega)$ are fourier transform of the body velocity $\mathbf{V}(t) = \dot{\boldsymbol{\xi}}(t)$ and wave amplitude at the origin $\eta(t)$, respectively. The governing equations of the linear BVP in frequency domain can then be derived and summarized as follows,

$$
\begin{cases}
\nabla^2 \phi = 0, & \mathbf{X} \in \Omega \\[2mm]
\dfrac{\partial \phi}{\partial z} - \dfrac{\omega^2}{g} \phi = 0, & \mathbf{X} \in \overline{S}_F : z = 0 \\[2mm]
\dfrac{\partial \boldsymbol{\phi}_R}{\partial \mathbf{n}} = \overline{\mathbf{n}}, \quad \dfrac{\partial (\phi_I + \phi_D)}{\partial \mathbf{n}} = 0, & \mathbf{X} \in \overline{S}_B \\[2mm]
\dfrac{\partial \phi}{\partial z} = 0, & \mathbf{X} \in S_D : z = -H
\end{cases}
\tag{4}
$$

where $\mathbf{X} = [x \ y \ z]^\mathsf{T}$ is the field point, $\mathbf{n}$ the normal vector at body surface pointing out of fluid, $\overline{\mathbf{n}} = [\mathbf{n}; \ \mathbf{r} \times \mathbf{n}]$, $\mathbf{r}$ is position vector on the body surface. According to Airy's wave theory, the incident wave propagating along positive X direction takes the form

$$
\phi_I(x,y,z,\omega) = \frac{ig}{\omega} \cdot \frac{\cosh[k(z+H)]}{\cosh(kH)} e^{ikx},
\tag{5}
$$

where k is the wave number satisfying the dispersion relation

$$
\omega^2 = gk \tanh(kH).
\tag{6}
$$

In addition, to guarantee the uniqueness of the solutions to Eq.4, the radiation conditions at infinity [18] are introduced:

$$
\lim_{x \to \pm\infty} \left(\frac{\partial \boldsymbol{\phi}_R}{\partial x} \mp ik\boldsymbol{\phi}_R \right) = 0, \quad \lim_{x \to \pm\infty} \left(\frac{\partial \phi_D}{\partial x} \mp ik\phi_D \right) = 0.
\tag{7}
$$

With the velocity potentials (Φ_I, Φ_R, and Φ_D), hydrodynamic pressure p can be obtained according to Bernoulli's equation (Eq.2) with the high-order term $\frac{1}{2}\rho(\nabla\Phi)^2$ neglected, and the hydrodynamic forces acting on the body can be determined

by integrating the pressure over the body surface $\overline{S}_B$. The total force/moment can be expressed as the sum of hydrostatic force/moment $\mathbf{F}_{HS}$, radiation force/moment $\mathbf{F}_R$, and wave excitation force/moment $\mathbf{F}_{Wt}$:

$$\mathbf{F}_{HS} = -\rho g \iint_{\overline{S}_B} z\overline{\mathbf{n}}\,dS = \mathbf{F}_B - \mathbf{K}_{HS}\boldsymbol{\xi}(t),$$

$$\mathbf{F}_R = -\rho \iint_{\overline{S}_B} \frac{\partial \Phi_R}{\partial t}\overline{\mathbf{n}}\,dS = -\frac{1}{2\pi}\int_{-\infty}^{\infty}\left[\boldsymbol{\lambda}(\omega)i\omega\overline{\mathbf{V}}(\omega) + \boldsymbol{\mu}(\omega)\overline{\mathbf{V}}(\omega)\right]e^{i\omega t}\,d\omega, \tag{8}$$

$$\mathbf{F}_{Wt} = -\rho \iint_{\overline{S}_B} \frac{\partial}{\partial t}(\Phi_I + \Phi_D)\overline{\mathbf{n}}\,dS = \Re\left\{\frac{1}{2\pi}\int_{-\infty}^{\infty}\overline{\eta}(\omega)\mathbf{F}_W(\omega)e^{i\omega t}\,d\omega\right\},$$

where $\mathbf{F}_B$ is static buoyance force which is balanced by gravitational force of the structure, $\mathbf{K}_{HS}$ the hydrostatic restoring stiffness, $\boldsymbol{\lambda}, \boldsymbol{\mu}$, and $\mathbf{F}_W$ denote the frequency-dependent added mass, radiation damping, wave excitation force transfer function matrices, respectively,

$$\boldsymbol{\lambda}(\omega) = \rho \iint_{\overline{S}_B} \overline{\mathbf{n}}\left[\boldsymbol{\phi}_R^{Re}\right]^{\mathsf{T}} dS,$$

$$\boldsymbol{\mu}(\omega) = -\rho\omega \iint_{\overline{S}_B} \overline{\mathbf{n}}\left[\boldsymbol{\phi}_R^{Im}\right]^{\mathsf{T}} dS, \tag{9}$$

$$\mathbf{F}_W(\omega) = -\rho i\omega \iint_{\overline{S}_B} (\phi_I + \phi_D)\overline{\mathbf{n}}\,dS.$$

The equations of motion of the floating platform built upon the hydrodynamic coefficients (Eq.9) are a set of linear equations:

$$\left\{-\omega^2\left[\mathbf{M} + \boldsymbol{\lambda}(\omega)\right] + i\omega\boldsymbol{\mu}(\omega) + \mathbf{K}_{HS}\right\}\overline{\boldsymbol{\xi}}(\omega) = \overline{\eta}(\omega)\mathbf{F}_W(\omega), \tag{10}$$

where $\mathbf{M}$ is the rigid-body mass of the platform. Despite the simplicity of the frequency-domain analysis approach, it cannot capture the nonlinear dynamic behavior and time transients of the system, which are crucial for the dynamic analysis of FWTs. In light of this, Cummins equation [19] is introduced which converts the frequency-domain equations (Eq.10) into a set of integro-differential equations with constant coefficients and convolution terms

$$\left[\mathbf{M} + \boldsymbol{\lambda}(\infty)\right]\ddot{\boldsymbol{\xi}}(t) + \int_0^t \mathbf{K}(t-\tau)\dot{\boldsymbol{\xi}}(\tau)d\tau + \mathbf{K}_{HS}\boldsymbol{\xi}(t) = \mathbf{F}_{Wt}, \tag{11}$$

where $\mathbf{K}(t)$ is the impulse response function representing the fluid memory effect:

$$\mathbf{K}(t) = \frac{2}{\pi}\int_0^{\infty}\boldsymbol{\mu}(\omega)\cos(\omega t)d\omega. \tag{12}$$

Numerical approach to solving the BVP: BEM

The Boundary Element Method, BEM, solution is based on Green's Theorem which transfers the computation region from the whole fluid domain to closed boundary surfaces. The free-surface Green function source potential $G(\mathbf{x},\mathbf{y})$ ($\mathbf{x}$: source point, $\mathbf{y}$: field point) which is introduced to derive the boundary integral equation automatically satisfies Laplace's Equation, free-surface, sea-bottom, and radiation boundary conditions (Eq. 4 except that on $\overline{S}_B$, and Eq.7). As a result, the integration region reduces to only the body surface $\overline{S}_B$ and thus significantly increase the computational efficiency. The reduced boundary integral equations take the form of

$$2\pi\phi_{Rj}(\mathbf{y}) + \iint_{\overline{S}_B}\phi_{Rj}(\mathbf{x})\frac{\partial G(\mathbf{x},\mathbf{y})}{\partial \mathbf{n}(\mathbf{x})}d\mathbf{x} = \iint_{\overline{S}_B}\overline{n}_j(\mathbf{x})G(\mathbf{x},\mathbf{y})d\mathbf{x},$$

$$2\pi\phi_D(\mathbf{y}) + \iint_{\overline{S}_B}\phi_D(\mathbf{x})\frac{\partial G(\mathbf{x},\mathbf{y})}{\partial \mathbf{n}(\mathbf{x})}d\mathbf{x} = -\iint_{\overline{S}_B}\frac{\partial \phi_I(\mathbf{x})}{\partial \mathbf{n}(\mathbf{x})}G(\mathbf{x},\mathbf{y})d\mathbf{x}, \tag{13}$$

where j denotes the platform motion in the j-th Dof. The mean wetted surface $\overline{S}_B$ can be approximated by a set of quadrilateral or triangular plane panels $\overline{S}_B \approx \sum_{l=1}^N s_l$, where $l = 1, 2, ..., N$, N denotes the number of panels and s_l denotes the surface of the l-th panel. The velocity potentials are assumed to be constant over each of the panels. In doing so, the boundary integral equations Eq. 13 can be discretized into a set of linear algebraic equations which enables a robust numerical solution method:

$$2\pi\phi_{Rj}(\mathbf{y}_r) + \sum_{l=1,l\neq r}^N \phi_{Rj}(\mathbf{x}_l)D_{rl} = \sum_{l=1,l\neq r}^N \overline{n}_j(\mathbf{x}_l)S_{rl},$$

$$2\pi\phi_D(\mathbf{y}_r) + \sum_{l=1,l\neq r}^N \phi_D(\mathbf{x}_l)D_{rl} = -\sum_{l=1,l\neq r}^N \frac{\partial \phi_I(\mathbf{x}_l)}{\partial \mathbf{n}(\mathbf{x})}S_{rl}, \tag{14}$$

where

$$D_{rl} = \iint_{s_l} \frac{\partial G(\mathbf{x}, \mathbf{y}_r)}{\partial \mathbf{n}(\mathbf{x})} d\mathbf{x}, \quad S_{rl} = \iint_{s_l} G(\mathbf{x}, \mathbf{y}_r) d\mathbf{x}. \tag{15}$$

With the solution of velocity potentials over all panels, the added mass, radiation damping and wave excitation force coefficients can be calculated using the discretized version of Eq. 9.

Analytical approach to solving the BVP
The simple geometry of a 2D rectangular platform submergence area allows us to divide the fluid domain into 3 regions as depicted in Fig.2. In doing so, a set of simplified BVPs with fewer inhomogeneous boundary conditions in each region are yielded and the analytical solution to the problem can be sought. However, the condition at the upper ($-d < z < 0$) and lower ($-H < z < -d$) parts of the same interface (e.g. $x = a$) are distinct. The exact analytical solution for this mixed boundary value problem only exists under very few cases [20]. The approximation approach of the weighted residuals method developed by Zheng et al. [15] is employed to obtain the analytical solution in this work.
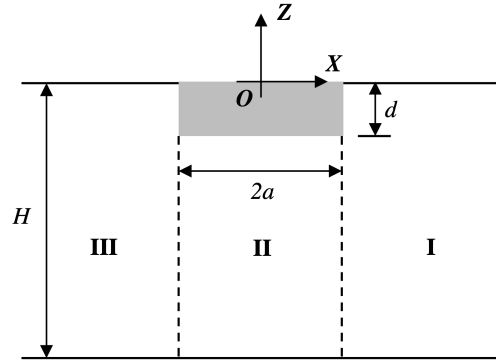

Figure 2: Sketch of the 2D rectangular platform in the OXZ plane with infinite length in the Y-axis.

The BVP of the radiation potential for pitch Dof in region II ($\phi_{R_{II}}^{pitch}$) is presented to demonstrate the analytical method. $\phi_{R_{II}}^{pitch}$ satisfies

$$
\begin{cases}
\dfrac{\partial^2 \phi_{R_{II}}^{pitch}}{\partial x^2} + \dfrac{\partial^2 \phi_{R_{II}}^{pitch}}{\partial z^2} = 0, & -H < z < -d, \ |x| < a \\[2mm]
\dfrac{\partial \phi_{R_{II}}^{pitch}}{\partial z} = -x & z = -d \\[2mm]
\dfrac{\partial \phi_{R_{II}}^{pitch}}{\partial z} = 0. & z = -H
\end{cases}
\tag{16}
$$

The general solution can be obtained by applying the method of separation of variables,

$$\phi_{R_{II}}^{pitch} = -\frac{(z+H)^2 x - x^3/3}{2(H-d)} + A_{20}x + B_{20} + \sum_{n=1}^{\infty} \left[A_{2n} e^{\beta_n(x+a)} + B_{2n} e^{-\beta_n(x-a)} \right] \cos\left[\beta_n(z+H)\right], \tag{17}$$

where $A_{20}, B_{20}, A_{2n}, B_{2n}$ are constant coefficients and $\beta_n = \pm\frac{n\pi}{H-d}$. By similar means, the radiation wave potentials in region I and III can be obtained and expressed as infinite series

$$
\begin{aligned}
\phi_{R_I}^{pitch} &= A_{10} e^{ik(x-a)} \cosh\left[k(z+H)\right] + \sum_{n=1}^{\infty} A_{1n} e^{-\kappa_n(x-a)} \cos\left[\kappa_n(z+H)\right], \\
\phi_{R_{III}}^{pitch} &= A_{30} e^{-ik(x+a)} \cosh\left[k(z+H)\right] + \sum_{n=1}^{\infty} A_{3n} e^{\kappa_n(x+a)} \cos\left[\kappa_n(z+H)\right],
\end{aligned}
\tag{18}
$$

where $A_{10}, B_{30}, A_{1n}, A_{3n}$ are constant coefficients, k the wave number determined by Eq.6 and κ_n is the eigenvalues defined by

$$\omega^2 = -g\kappa_n \tan(\kappa_n H). \tag{19}$$

To determine the unknown coefficients of the orthogonal series in Eq.17 and 18, the continuity conditions of the pressure and normal velocity between two neighboring regions ($x = \pm a$) are imposed. Take the interface between region I and II ($x = a$) as example, continuity conditions for the radiated potentials in the pitch Dof can be expressed as

$$\int_{-H}^{-d} \phi_{R_I}^{pitch}\Big|_{x=a} \cos\left[\beta_n(z+H)\right] dz = \int_{-H}^{-d} \phi_{R_{II}}^{pitch}\Big|_{x=a} \cos\left[\beta_n(z+H)\right] dz,$$

$$\int_{-H}^{0} \frac{\partial \phi_{R_I}^{pitch}}{\partial x}\Big|_{x=a} \cos\left[\kappa_n(z+H)\right] dz = \int_{-d}^{0} z\cos\left[\kappa_n(z+H)\right] dz + \int_{-H}^{-d} \frac{\partial \phi_{R_{II}}^{pitch}}{\partial x}\Big|_{x=a} \cos\left[\kappa_n(z+H)\right] dz. \tag{20}$$

Once all unknown coefficients are determined, the radiated and diffracted potentials can be obtained from Eq.17–18.

AERO-HYDRO-ELASTIC-CONTROL MODELING IN SIMULINK

The FWT is a complex mechanical system including multiple components of blades, hub, nacelle, tower, floating platform and moorings which are subjected to wind and wave loads, as well as components of generator and gearbox which operate under the regulation of the control system. MATLAB/Simulink provides a general multibody simulation package, Simscape/Multibody, which allows for the implementation of rigid and deformable body dynamics, the computation of aerodynamic and hydrodynamic loads and can be integrated with other Simulink modules for the application of control laws. Moreover, Simulink features visualization capability for 3D modeling and response. The topology of a generic FWT model in Simulink proposed in this work is illustrated in Fig.3.
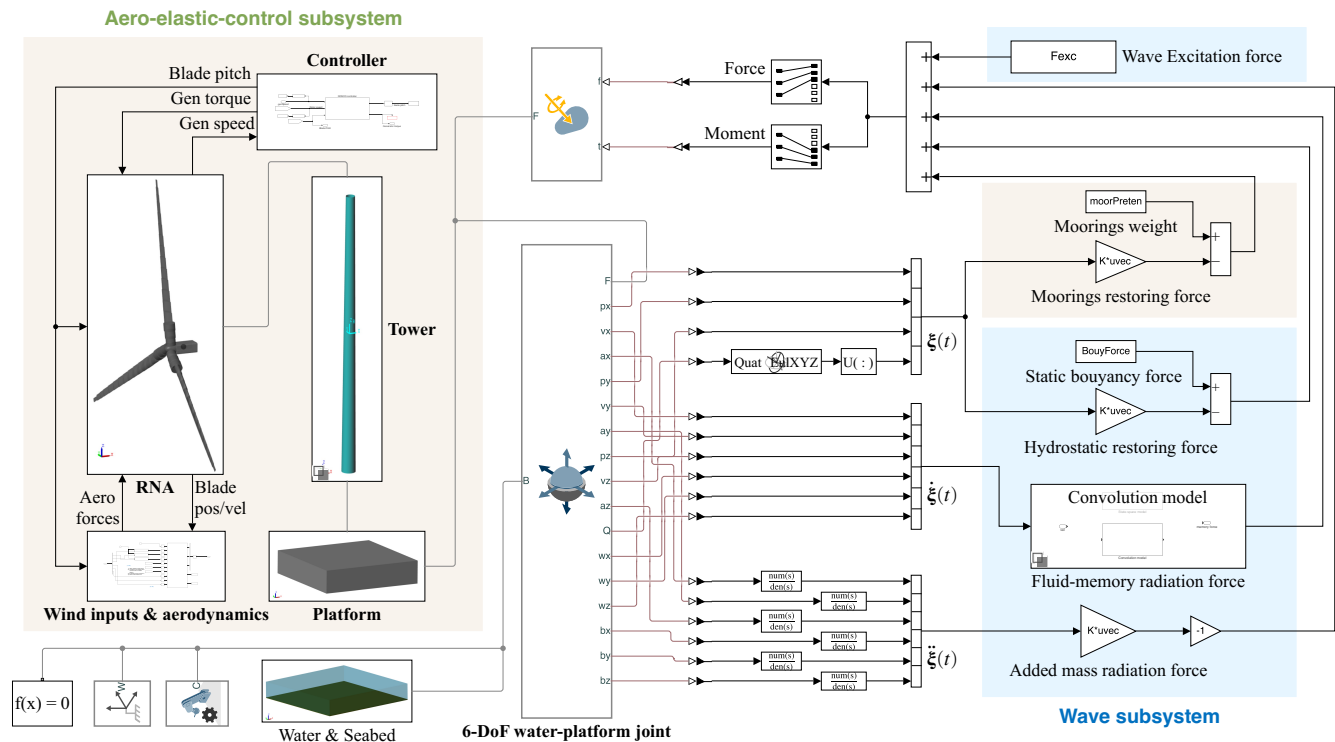

Figure 3: Topology of a generic floating wind turbine developed in MATLAB/Simulink environment.

The world frame (inertia coordinate system) is defined on the still water surface. A 6-Dof joint is used to define the 3D movements of the floating platform with respect to the world frame. The hub, nacelle, and floating platform that have relatively small internal deformation can be modeled as rigid bodies with the lumped mass and inertia being defined at their centers of mass (CoM). The tower and blades deformabilities are not taken into account in present work. They are therefore modeled as an assembly of rigid bodies with distributed mass and inertia properties. In the rotor-nacelle assembly (RNA), the low-speed shaft is at one end connected to the blades which are free to rotate under wind actions, and at the other end connected to the generator via a gearbox. The rotational speed of the generator is measured and fed into the controller which then outputs the blade pitch

and generator torque commands to regulate the power generation following the ROSCO control strategy. A series of sensors are deployed along the blade to measure the instantaneous position and velocity at different blade cross-sections with respect to the world frame. The blade position signals are transferred to the wind inputs and aerodynamics subsystem to interpolate the inflow wind velocities felt on the blade sections from a grid of spatial wind field generated by TurbSim [21]. The inflow wind velocities, blade velocities as well as blade pitch angle are then passed to the aerodynamic computation function, which adopts the unsteady blade/element momentum method to evaluate the aerodynamic forces applied on each blade sections.

The wave-body interaction effects can be determined by solving the linear BVP numerically or analytically. In order for the time-domain integration of the wave subsystem with the remaining FWT system, the direct results of the frequency-dependent hydrodynamic coefficients $\boldsymbol{\lambda}(\omega), \boldsymbol{\mu}(\omega), \boldsymbol{F}_W(\omega)$ obtained from both methods are converted to the infinite-frequency added mass $\boldsymbol{\lambda}(\infty)$, fluid-memory impulse response function $\mathbf{K}(t)$ and wave excitation force $\mathbf{F}_{Wt}(t)$ according to Cummins equation (Eq.11). The infinite-frequency added mass is represented as a matrix as shown in Fig.3, which is multiplied by the platform acceleration $\ddot{\boldsymbol{\xi}}(t)$ to get the added-mass radiation force. The fluid-memory impulse response function (Eq.12) is imported in the convolution integral model coded in a Matlab function block as shown in Fig.3, which receives the platform velocity $\dot{\boldsymbol{\xi}}(t)$ to calculate the fluid-memory radiation force. The integral is calculated up to a specified time horizon to enhance the computational efficiency. The hydrostatic and moorings restoring effects are both modeled with stiffness matrices, which are multiplied by the platform displacement $\boldsymbol{\xi}(t)$ to get the restoring forces. The wave excitation force is calculated by the inverse Fourier transform given the wave amplitude $\overline{\eta}(\omega)$ as presented in Eq.8, and is imported as time-series data in the Simulink model. The aforementioned forces as well as the weight of moorings and displaced water by the platform are summed and applied to the 6-DoF water-platform joint as shown in Fig.3. After building the full system and specifying wind and wave inputs, the time-domain dynamic analysis can be carried out by solving the equations of motion numerically using Simulink inbuilt ODE solvers.

EXAMPLE AND DISCUSSIONS

An example of the 5-MW ITIBarge FWT [22] is taken to evaluate the Simulink modeling approach by comparing the results against those calculated from a popular FWT simulation code, OpenFAST (v3.2.1). The wave-platform interaction effect can be determined by either the open-source BEM code, Nemoh, or the analytical method. The analytical model is developed using the MATLAB/Symbolic Math Toolbox. The width of the ITIBarge cross-section is $2a = 40\ m$, draft $d = 4\ m$ and the water depth $H = 150\ m$. The first 10 terms in the eigenfunctions of radiation and diffraction potentials at each region (e.g., 17,18 for the radiation problem in pitch DoF) are taken to calculate the potential functions in the analytical method. In order to obtain the pseudo-2D results from the 3D BEM code Nemoh, the out-of-plane length (along Y-axis) of the platform is taken as 20 times its width ($800m$ in total). The analytical results are correspondingly multiplied by that length in Y-axis. The comparison between the analytical and Nemoh's results in terms of the impulse response function $\mathbf{K}(t)$ (Eq.12) and wave excitation force $\mathbf{F}_W(\omega)$ (Eq.9) is illustrated in Fig.4 (a) and (b), respectively. It can be found that the results calculated from both methods agree well which indicates the accuracy of the analytical method. Nemoh suffers from numerically induced oscillations at certain frequencies, whereas the analytical method tends to give results that are less prone to numerically induced noise.
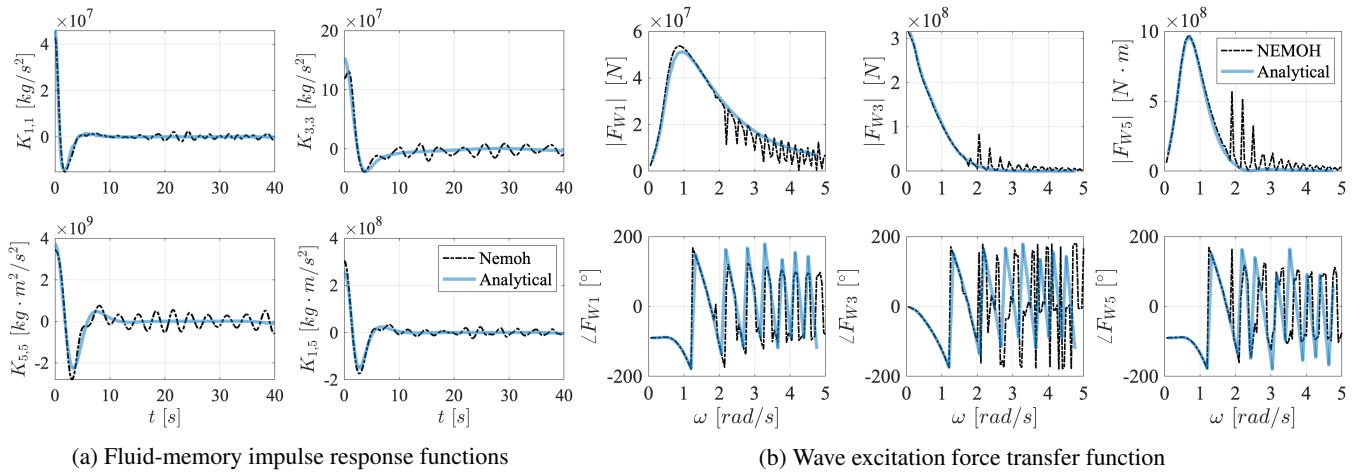

(a) Fluid-memory impulse response functions

(b) Wave excitation force transfer function

Figure 4: Comparison of the impulse response functions $\mathbf{K}(t)$ and wave excitation force transfer function $\mathbf{F}_W(\omega)$ in surge–1, heave–3 and pitch–5 DoFs calculated from Nemoh and analytical methods.

Only the 3 platform DoFs of surge, heave and pitch are activated in both Simulink and OpenFAST models to investigate the planar dynamic response of the full FWT system. The ITIBarge platform is moored with 8 catenary mooring lines. Their weight and restoring stiffness are obtained from the quasi-static mooring analysis code, MAP++ [23], and are imported in both Simulink and OpenFAST models. Cummins equation (Eq.11) is adopted in OpenFAST to determine the hydrodynamic loads, with the time horizon of the convolution integral being set the same as that in the Simulink model ($0 \sim 40s$). The infinite-frequency added masses, fluid-memory impulse response functions and wave excitation force transfer functions obtained from Nemoh and analytical method are imported in the Simulink model, which are labeled as "Simulink-Nemoh" and "Simulink-Analytical", respectively. Nemoh's results are imported in OpenFAST, which is taken as the benchmark and labeled as "OpenFAST-Nemoh". In addition, the computation methods to evaluate the aerodynamics and controls in OpenFAST are set to be consistent with those employed in the Simulink model. In this case, the comparison between "Simulink-Nemoh" and "Simulink-Analytical" models demonstrates the effects of different hydrodynamic approaches on the system behavior, and the comparison between "OpenFAST-Nemoh" and "Simulink-Nemoh" models can be used to examine the implementation of FWT modeling in Simulink.

A steady wind field of $8m/s$ which is constant over time is applied to both models. The JONSWAP wave spectrum [22] with the significant wave height of $2m$, peak-spectral period of $10s$, wave direction along X-axis and frequency limit of 0–10 rad/s is set in OpenFAST to generate random wave amplitude time series (see Fig.5). In light of the good agreement of the wave excitation transfer functions between the analytical and Nemoh results as shown in Fig.4(b), the wave excitation forces calculated from the wave series in OpenFAST are directly imported to the Simulink model. The time series of wave excitation force in pitch DoF is shown in Fig.5. The platform pitch rotation of both the OpenFAST model and Simulink model are also depicted in Fig.5, which shows well agreement among the three models. The operation conditions of the turbine for three models are compared in Fig.6. The good match of rotor speed Ω_r, aerodynamic torque T_{aero} and mechanical power generation P demonstrates the accurate implementation of the aerodynamic force and controller in Simulink compared to OpenFAST. The overall agreement in the three models verifies the ability of the developed Simulink model to predict the dynamic behavior of FWTs using either numerical or analytical hydrodynamic modeling approaches.
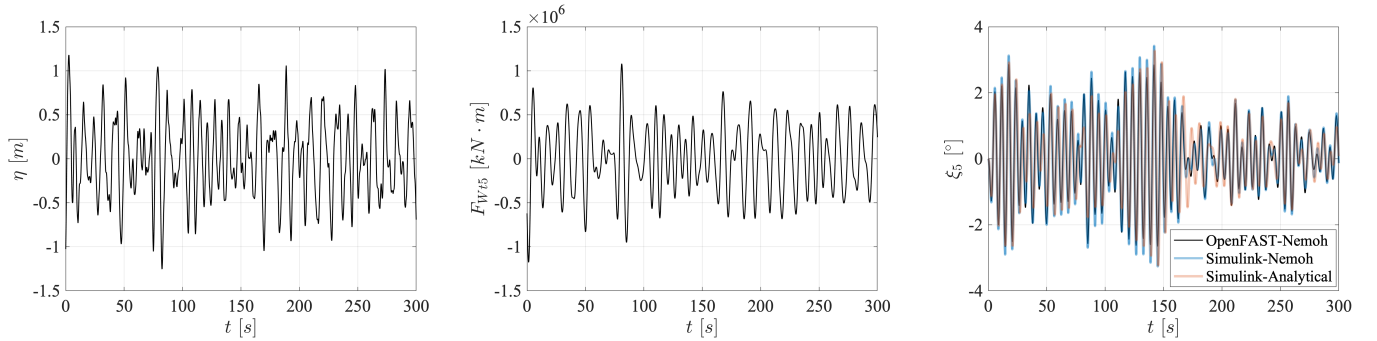

Figure 5: Wave elevation η, wave excitation force in Pitch DoF F_{Wt5} and platform pitch rotation ξ_5 for different models.
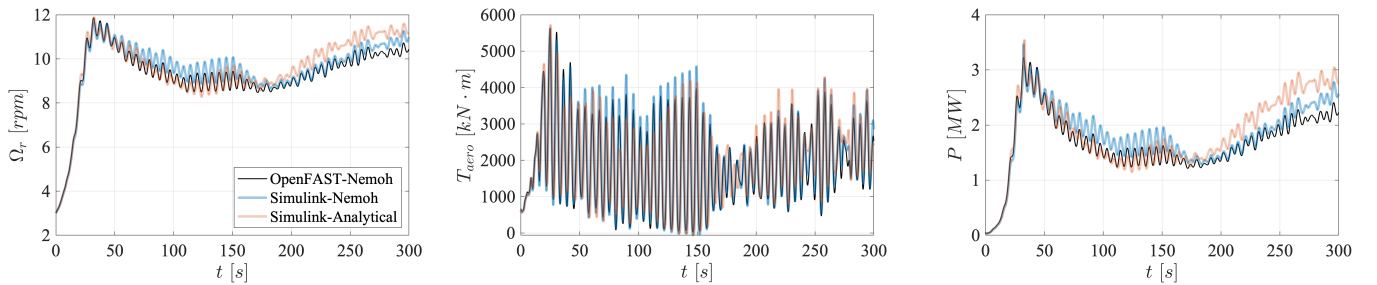

Figure 6: Rotor speed Ω_r, aerodynamic torque T_{aero} and mechanical power P obtained from different models.

Fig.7 illustrates the wave elevation η, aerodynamic torque T_{aero} and platform pitch rotation ξ_5 from the "Simulink-Analytical" model in the frequency domain. The predominant frequency of the wave excitation f_{wave}, natural frequency of the system in pitch DoF f_{pitch} and the blade rotational speed and its multiples f_{1P}, f_{2P}, f_{3P} are also annotated. The platform movements

modify the relative wind velocity felt by the blades and thus lead to peaks at f_{wave} and f_{pitch} in the aerodynamic torque, which also explains the occurrence of f_{1P}, f_{2P}, f_{3P} effects even under the steady wind excitation. However, due to the large inertia difference between the platform and the rotor, the platform motion is hardly affected by the loads from the rotor.
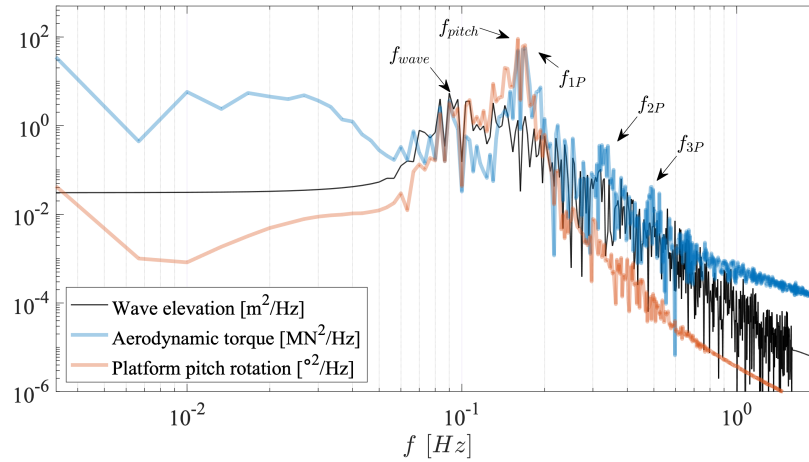

Figure 7: Wave elevation, aerodynamic torque and platform pitch rotation in the frequency domain.

CONCLUSIONS

A new simulation framework for the dynamic modeling of FWTs is developed in this work. An analytical wave-platform interaction model is developed in the Symbolic Math Toolbox in MATLAB. The open-source BEM code, Nemoh, is taken as a benchmark evaluation of the analytical method. The hydrodynamic coefficients obtained from the analytical method agree well with those calculated from Nemoh and are free from the numerically induced noise. An implementation scheme involving the structural modeling, aerodynamics and controls using Simscape/multibody and other extensive Simulink libraries is proposed in this work. The wave subsystem includes the additional hydro-related mass and stiffness matrices and fluid-memory convolution integrals calculated from either the analytical method or Nemoh, and is integrated with the remaining FWT system. The Simulink model is validated against OpenFAST by examining the example of a 5 MW ITIBarge FWT with rigid blades and tower under steady wind and stochastic wave. In both Simulink and OpenFAST models only the planar DoFs of surge, heave and pitch are activated and the out-of-plane length of the platform is taken sufficiently long to adapt to the implementation of the 2D analytical model. The Simulink model shows good agreement with OpenFAST in terms of the aerodynamic and hydrodynamic loads, controller behavior as well as platform response, which indicates Simulink model's capability to carry out robust dynamic analysis of FWTs. Future works will demonstrate the effects occurring from the flexibility of tower and blades.

REFERENCES

[1] IRENA, World energy transitions outlook 2022: 1.5°C pathway (2022).

[2] Wind Energy Generation Systems Part 3-2: Design Requirements for Floating Offshore Wind Turbines, IEC TS 61400-3-2:2019 (2019).

[3] B. Skaare, F. G. Nielsen, T. D. Hanson, R. Yttervik, O. Havmøller, A. Rekdal, Analysis of measurements and simulations from the hywind demo floating wind turbine, Wind Energy 18 (6) (2015) 1105–1122.

[4] A. Jacobsen, M. Godvik, Influence of wakes and atmospheric stability on the floater responses of the hywind scotland wind turbines, Wind Energy 24 (2) (2021) 149–161.

[5] Openfast documentation, version v3.2.0, https://openfast.readthedocs.io/en/main/, accessed: 2022-10-01.

[6] Using sesam and bladed in one workflow, DNV GL (2020).

[7] Hawc2 info, https://www.hawc2.dk/hawc2-info, accessed: 2022-10-01.

[8] J. Jonkman, W. Musial, Offshore code comparison collaboration (OC3) for iea wind task 23 offshore wind technology and deployment, Tech. rep., National Renewable Energy Lab.(NREL), Golden, CO (United States) (2010).

[9] A. Robertson, J. Jonkman, F. Vorpahl, W. Popko, J. Qvist, L. Frøyd, X. Chen, J. Azcona, E. Uzunoglu, C. Guedes Soares, et al., Offshore code comparison collaboration continuation within iea wind task 30: Phase II results regarding a floating semisubmersible wind system, in: International Conference on Offshore Mechanics and Arctic Engineering, Vol. 45547, American Society of Mechanical Engineers, 2014, p. V09BT09A012.

[10] A. N. Robertson, F. Wendt, J. M. Jonkman, W. Popko, H. Dagher, S. Gueydon, J. Qvist, F. Vittori, J. Azcona, E. Uzunoglu, et al., Oc5 project phase II: validation of global loads of the deepcwind floating semisubmersible wind turbine, Energy Procedia 137 (2017) 38–57.

[11] L. Wang, A. Robertson, J. Jonkman, Y.-H. Yu, Oc6 phase I: Improvements to the openfast predictions of nonlinear, low-frequency responses of a floating offshore wind turbine platform, Renewable Energy 187 (2022) 282–301.

[12] Wamit, inc. the state of the art in wave ineraction analysis., `https://www.wamit.com/`, accessed: 2022-10-01.

[13] ANSYS, Aqwa theory manual (2015).

[14] Nemoh, `https://github.com/LHEEA/Nemoh`, accessed: 2022-10-01.

[15] Y. Zheng, Y. You, Y. Shen, On the radiation and diffraction of water waves by a rectangular buoy, Ocean engineering 31 (8-9) (2004) 1063–1082.

[16] M. Hansen, Aerodynamics of wind turbines, Routledge, 2015.

[17] Rosco documentation, version v2.6.0, `https://rosco.readthedocs.io/en/latest/`, accessed: 2022-10-01.

[18] J. V. Wehausen, The motion of floating bodies, Annual review of fluid mechanics 3 (1) (1971) 237–268.

[19] W. Cummins, W. Iiuhl, A. Uinm, The impulse response function and ship motions (1962).

[20] D. G. Duffy, Mixed boundary value problems, Chapman and Hall/CRC, 2008.

[21] Turbsim, `https://www.nrel.gov/wind/nwtc/turbsim.html`, accessed: 2022-10-01.

[22] J. M. Jonkman, Dynamics modeling and loads analysis of an offshore floating wind turbine, University of Colorado at Boulder, 2007.

[23] Map++, `https://www.nrel.gov/wind/nwtc/map-plus-plus.html`, accessed: 2022-10-01.